Neurobiology of Disease 93 (2016) 172–183

Contents lists available at ScienceDirect

Neurobiology of Disease

journal homepage: www.elsevier.com/locate/ynbdi

Reelin-immunoreactive neurons in entorhinal cortex layer II selectively express intracellular amyloid in early Alzheimer's disease

Asgeir Kobro-Flatmoen, Anne Nagelhus, Menno P. Witter *

Kavli Institute for Systems Neuroscience & Centre for Neural Computation, Norwegian University of Science and Technology (NTNU), Trondheim, Norway

ARTICLE INFO

Article history:
Received 6 April 2016
Revised 6 May 2016
Accepted 13 May 2016
Available online 16 May 2016

Keywords:
Neurodegeneration
Neuropathology
Amyloid-β
Hippocampal formation
Parahippocampal region

ABSTRACT

The onset of Alzheimer's disease (AD) is associated with subtle pathological changes including increased intracellular expression of amyloid-β (Aβ). A structure affected particularly early in the course of AD is the entorhinal cortex, where neuronal death in layer II is observed already at initial stages. Neurons in EC-layer II, particularly those that express the protein Reelin, give rise to projections to the hippocampal dentate gyrus and this projection shows severe loss of synaptic contacts during early-stage AD. Given this anatomical specificity, we sought to determine whether increased intracellular expression of Aβ is selectively associated with Reelin-immunoreactive neurons in layer II of the entorhinal cortex. Here we report that in a transgenic rat model, which mimics the onset and distribution of extracellular amyloid deposits seen in human AD subjects, expression of intracellular Aβ in entorhinal layer II selectively occurs in Reelin-immunoreactive neurons during the early, pre-plaque stage. This Reelin-Aβ association is also present in human subjects with AD-related pathological changes, even in early disease stages. These findings strongly indicate that Reelin-immunoreactive neurons in entorhinal layer II play a crucial role during the initial stages of AD, and may therefore lead to refined hypotheses concerning the origin of this devastating condition.

1. Introduction

Alzheimer's disease (AD) causes progressive cognitive impairment with loss of explicit memory, as measured with cued recall, as one of the most characteristic early features (Dubois et al., 2014). The AD-brain contains characteristic pathological changes which include abundant extra-cellular amyloid deposits, called plaques, a multitude of neurofibrillary tangles and massive neuronal loss (Duyckaerts et al., 2009). Importantly, the pathology is not indiscriminately present throughout the brain, such that associational cortical areas, in particular in the temporal lobes are particularly affected (Braak and Braak, 1991; Hyman and Trojanowski, 1997). This points to regional differences in vulnerability to underlying disease-mechanisms.

A potential key player in AD is amyloid-β (Aβ). This small aggregation-prone peptide, ranging in size from 37 to 43 amino acids, originates from sequential cleavage of the amyloid precursor protein (APP) by β- and γ-secretase. In its fibrillar, insoluble form, Aβ is a major constituent of the extracellular plaques associated with later disease stages (Thal et al., 2000). Inside neurons, the amount of soluble Aβ is already increased at early, prodromal stages of the disease (D'Andrea et al., 2001; Fernandez-Vizarra et al., 2004; Gouras et al., 2000, 2010; Pensalfini et al., 2014). The correlation between the amount of amyloid deposits with cognitive decline appears weak (Arriagada et al., 1992). In contrast, the expression of soluble intracellular Aβ (iAβ) in the cortex correlates well with dementia status (McLean et al., 1999; Naslund et al., 2000). The latter finding is corroborated by reports that in transgenic animal models memory deficits are present when iAβ but no extracellular Aβ is detectable (Billings et al., 2005; Iulita et al., 2014; Knobloch et al., 2007; Leon et al., 2010). Also, clearance of iAβ reverses memory impairments (Billings et al., 2005), and increased amounts of iAβ correlate well with neuronal loss (Casas et al., 2004; Cohen et al., 2013; Umeda et al., 2011). A direct link to impaired neuronal functioning has also been found, as soluble Aβ disrupts synaptic plasticity and inhibits long-term potentiation both in vitro (Lambert et al., 1998) and in vivo (Walsh et al., 2002). Finally, in a 3D cell-culture system harboring neurons transfected with familial AD mutations, Aβ-accumulation reversibly induces hyperphosphorylation and aggregation of tau (Choi et al., 2014). Taken together, soluble iAβ thus seems to be a key player in the initiation of the disease-cascade which eventually culminates in the characteristic pathological and cognitive changes seen in AD.

The seminal histopathological study on AD by Braak and Braak (1991) revealed that initial changes related to formation of neurofibrillary tangles occur in layer II of lateral parts of the entorhinal cortex (EC) at the border with the perirhinal cortex. It has since been established

* Corresponding author at: Kavli Institute for Systems Neuroscience & Centre for Neural Computation, Faculty of Medicine, NTNU, Postboks 8905, No-7491 Trondheim, Norway.
E-mail addresses: asgeir.kobro-flatmoen@ntnu.no (A. Kobro-Flatmoen), anne.nagelhus@ntnu.no (A. Nagelhus), menno.witter@ntnu.no (M.P. Witter).
Available online on ScienceDirect (www.sciencedirect.com).

http://dx.doi.org/10.1016/j.nbd.2016.05.012

that EC is also subject to extracellular amyloid depositions from an early stage of the disease (Thal et al., 2000). Further, massive neuronal loss in EC-layer II characterizes early AD (Gomez-Isla et al., 1996), a feature also evident in at least a subset of subjects with mild cognitive impairment (Kordower et al., 2001), of which the majority are likely to convert to AD (Espinosa et al., 2013; Grundman et al., 2004). Clearly, these findings implicate EC, and particularly the neurons in layer II, in the onset of AD.

Neurons in EC-layer II give rise to the main projection to the hippocampal dentate gyrus (DG) and this projection shows severe loss of synaptic contacts during early-stage AD (Scheff et al., 2006). Many principal neurons in EC-layer II in mammals express Reelin (Chin et al., 2007; Herring et al., 2012; Kitamura et al., 2014; Martinez-Cerdeno et al., 2003; Perez-Garcia et al., 2001; Pesold et al., 1998; Ramos-Moreno et al., 2006). Such a Reelin-expressing population in superficial layers is atypical for cortex, where Reelin is expressed primarily in a subset of principal cells of layer V (Pesold et al., 1998; Ramos-Moreno et al., 2006). In rodents, Reelin-expressing neurons in EC-layer II, as established by their Reelin-immunoreactivity (Reelin-IR), form the sole origin of the excitatory projection to DG (Berndtsson, 2013; Gianatti, 2015; Kitamura et al., 2014; Varga et al., 2010), which is of interest since Reelin is a modulatory protein involved in synaptic plasticity (Qiu et al., 2006; Rogers et al., 2011; Weeber et al., 2002).

We thus chose to focus on EC and hypothesized that the population of Reelin-IR neurons in layer II is particularly vulnerable to accumulation of iAβ. We utilized the McGill-R-Thy1-APP rat model for AD, which faithfully mimics the onset and distribution of extracellular amyloid deposits seen in human AD subjects, and has an extended phase of iAβ-accumulation (Iulita et al., 2014; Leon et al., 2010). Our data show that Reelin-IR neurons in EC-layer II selectively stain positive for iAβ during the early, pre-plaque stage. Furthermore, we show that this Reelin-Aβ association is present in human subjects having AD-related pathology, not only in the late stages but also in early stages, suggesting that Reelin-IR neurons in EC-layer II play a crucial role during the initial events leading to AD.

2. Materials and methods

2.1. Experimental design

In this paper we aimed to test whether accumulation of iAβ in EC-layer II specifically occurs in Reelin-IR neurons. For the experimental part of this study we used the McGill-R-Thy1-APP homozygous transgenic rat model (Heggland et al., 2015; Leon et al., 2010). Animals carry a transgene containing human *APP751* with the Swedish double- and Indiana mutations expressed under the murine Thy1.2 promoter. All rats were bred at the Kavli Institute for Systems Neuroscience, at the Norwegian University of Science and Technology. Experimental protocols were approved by the Norwegian Animal Research Authority and are in accordance with the European Convention for the Protection of Vertebrate Animals used for Experimental and Other Scientific Purposes. We used 20 animals divided into four age-groups ($n = 5$/group), postnatal day 15 (5 males), 1 month (3 males and 2 females), 3 months (3 males and 2 females), and 6 months (3 males and 2 females). To corroborate the findings in the rat model, we used sections through EC from AD-subjects with pathologically verified Braak stages I (female, 83 years old), III (female, 75 years old) and V (male, 66 years old) (Braak and Braak, 1991). These sections were provided by Professor Ricardo Insausti (University of Castilla-La Mancha, Spain) and originally consisted of three sections from each of three subjects, approximately equally distributed along the anteroposterior extent of EC. After optimization of the staining-protocols we were left with two sections from Braak stage I, and one section from each of stages III and V, on which the double-IHC experiments were carried out. In the case of the two sections for Braak stage I, these were from an anterior and a posterior level, while in the case of Braak stages III and V, the sections were taken at a middle or posterior level, respectively.

2.2. Genotyping

The animals were genotyped for the expression of the transgene by quantitative PCR (qPCR), as previously described (Heggland et al., 2015). We used genomic DNA isolated from ear tissue with a High Pure PCR Template Preparation Kit (Roche Diagnostics, Basel, Switzerland). RT^2 qPCR Primer Assays from Qiagen (Venlo, Netherlands) were used to detect the transgene (human AβPP) and a normalization gene (GAPDH or beta-actin) with FastStart Universal SYBR Green Master (Roche Diagnostics) on an Applied Biosystems StepOnePlus real-time PCR system (Life Technologies Ltd., Thermo Fisher Scientific, Waltham, MA, USA). From the qPCR, $\Delta\Delta C_T$ values were calculated with a known homozygous sample as reference (Livak and Schmittgen, 2001).

2.3. Tissue processing and IHC

Animals were anesthetized using isoflurane gas (Abbott Lab., Cat# 05260-05) followed by intraperitoneal injection of pentobarbital (Norwegian Pharmacy Association, Cat# 306498). Subsequently, transcardial perfusion was carried out with a Ringer's Solution (145 mM NaCl, VWR Int. LLC, Cat# 27800.291; 3.35 mM KCl, Millipore, Cat# 1.04936.1000; 2.38 mM $NaHCO_3$, Millipore, Cat# 1.06329.1000) at pH 6,9, followed by circulation of 4% freshly depolymerized paraformaldehyde-solution (Millipore, Cat# 1.04005.1000) in phosphate buffer (PB: purified de-ionized water with di-sodium hydrogen phosphate dihydrate, Millipore, Cat# 1.37036.500, mixed with sodium di-hydrogen phosphate monohydrate, Millipore, Cat# 1.06346.1000, at 125 mM, pH 7.6; note that this applies to all uses of PB) for 2–3 min. The brains were removed and post fixed in the same fixative overnight, then placed in 2% DMSO solution (dimethyl sulfoxide, VWR Int. LLC, Cat# 23486.297, in PB and 20% glycerine, VWR, Cat# 24387.292) in a refrigerator until sectioning. Brains were sectioned at 40 μm in the coronal plane with a freezing microtome (Microm HM430, Thermo Fisher Scientific, Waltham, MA, USA). For each animal, we collected six series of equally spaced sections. One series was used (i.e. 40 μm sections with a 200 μm spacing), and immunohistochemistry was done on free-floating sections. Heat Induced Antigen Retrieval was carried out on all tissue at 60 °C for 3 h in PB.

2.4. Rat tissue

For fluorescent immunolabeling of rat-tissue, blocking with 5% goat serum (Abcam, Cat# AB7481) in PB was carried out for 2 h. For immunoenzyme staining of rat tissue, incubation with ready-to-use hydrogen peroxide (Thermo Scientific, Cat# TA-012-HP) was carried out for 10 min followed by incubation with Ultra V Block (Thermo Scientific, Cat# TA-012-UB) for 10 min and finally incubation with 5% goat serum in PB for 1 h. Subsequently, co-incubation with primary antibodies in PB (for immunofluorescence) or Tris buffered saline (for immunoenzyme-staining: TBS; purified de-ionized water with 50 mM Tris, Millipore, Cat# 1.08382; 150 mM NaCL, VWR Int. LLC; pH adjusted to 8.0 using hydrochloric acid, Millipore, Cat# 1.00317), both solutions containing 0.5% Triton X-100 (Millipore, Cat# 1.08603.1000) and 5% goat serum, was carried out in the following order: Rabbit anti-Reelin (1:50 for fluorescence/1:600 for immunoenzyme-staining, Biorbyt, Cat# Orb11331, RRID AB_10750301) with Mouse anti-Aβ McSA1 (1:1000, Medimabs, Inc., Cat# MM0015-P, RRID: AB_1807985); Rabbit anti-Reelin (1:50, Biorbyt) with Mouse anti-Aβ MOAB-2 (1:500, Biosensis, Cat# M-1586-100); Rabbit anti-Reelin (1:50, Biorbyt) with Mouse anti-Reelin G10 (1:500, Millipore, Cat# MAB5364, RRID: AB_2179313); Goat anti-Reelin (1:200, R&D Systems, Cat# AF3820, RRID AB_2253745) with Mouse anti-Aβ McSA1 (1:1000, Medimabs, Inc.); Mouse anti-Reelin G10 (1:1000, Millipore) with Rabbit anti-Aβ42 (1:500, IBL Ltd., Cat#

18582). For immunofluorescence, secondary antibodies were purchased from Life Technologies and included Alexa 488 Goat anti-Rabbit (Cat# A11008, RRID: AB_10563748), Alexa 546 Goat anti-Mouse (Cat# A11003, RRID: AB_10562732) and Alexa 488 Donkey anti-Goat (Cat# A11055, RRID AB_10564074). For fluorescence, all sections were incubated with secondary antibodies in 1:350 dilution with PB containing 0.5% Triton X-100 and 5% goat serum. Each pair of secondary antibodies was applied simultaneously for 2 h at room temperature, with one exception: in the double-immunofluorescence staining with Goat anti-Reelin and McSA1 (see Fig. 5B) the tissue was first incubated with Alexa 488 Donkey anti-Goat for 1 h, then washed, and then incubated with Alexa 546 Goat anti-Mouse for 1 h. For immunoenzyme-staining of rat tissue, we used as secondary antibodies AP-conjugated goat anti-mouse polymer (Biocare, Cat# MALP521L) and HRP-conjugated goat anti-rabbit polymer (Dako, Cat# K4011), both ready-to-use reagents. The secondary antibodies were visualized using enzymatic chromogens, and the incubation was conducted under close visual inspection until a satisfactory color-contrast was achieved. Chromogens included Dako DAB + (Dako, Cat#K4011) for HRP-conjugated goat anti-rabbit polymer (dilution according to the manufacturer's instruction, incubation time approximately 10 min) followed by Ferangi Blue (Biocare Medical, Cat# FB813S) for the AP-conjugated goat anti-mouse polymer (dilution 1:300, incubation time approximately 5 min). Processed tissue was mounted on glass slides from a solution of 50 mM tris(hydroxymethyl)aminomethane (Millipore, Cat# 1.08382.1000) with hydrochloric acid, at pH 7.6, containing gelatin (Oxoid, Ltd. Cat# LP0008), and then left to dry overnight before being coverslipped using entellan (Merck KGaA, Cat# 1.07960.0500).

2.5. Human tissue

The human-tissue was initially incubated with Dual-Block reagent (Dako Cat# S2003) for 10 min followed by incubation with 10% goat serum in PB for 1 h. Subsequently, co-incubation with primary antibodies in PB containing 0.4% Saponin (VWR, Cat# 27534.187) and 5% goat serum was carried out, using Rabbit anti-Reelin (1:50, Biorbyt) with Mouse anti-Aβ McSA1 (1:150, Medimabs). As secondary antibodies we used AP-conjugated goat anti-mouse polymer (Biocare, Cat# MALP521L) and HRP-conjugated goat anti-rabbit polymer (Dako, Cat# K4011), both ready-to-use reagents. The secondary antibodies were visualized using enzymatic chromogens, and the incubation was conducted under close visual inspection until a satisfactory color-contrast was achieved. Chromogens included AEC (Dako, Cat# K3469) for the HRP-conjugated goat anti-rabbit polymer (incubation time approximately 5 min) followed by Ferangi Blue (Biocare Medical) for the AP-conjugated goat anti-mouse polymer (dilution 1:125, incubation time approximately 10 min).

Table 1 contains an overview of the primary and secondary antibodies used in this study.

2.6. Microscopy and stereology

For the rat model, we randomly selected one of the six series of sections from each brain, such that the full extent of EC was represented for each animal. Layer II of LEC and MEC was delineated in Stereo Investigator (MicroBrightField Inc.) following established criteria (Kjonigsen et al., 2011) under dark field illumination (Axio Imager M1 microscope, Carl Zeiss). Analysis of co-localization was carried out using Stereo Investigator, applying the principles of stereology, which have been described in detail previously (West et al., 1991). Briefly, using epifluorescence microscopy (Zeiss Axio Imager M1), neurons were identified in a systematically randomized manner by applying a predefined virtual grid where each intersection contains a counting frame. Each neuron contained within a counting frame according to the stereological principles for inclusion was analyzed to determine if it was positive for Reelin and/or iAβ, by focusing through the tissue within a virtual dissector frame using a high power objective (100× oil, N.A. 1.4). Confocal images were obtained with the use of a Zeiss LSM Meta 510 confocal microscope, using Zen software (Carl Zeiss, Version 6,0,0303) with a 100× oil immersion objective (N.A. 1.4). Confocal images were subsequently color coded using the lookup table in ImageJ (NIH, Version 1.43 m).

We tested for normality of distribution, homogeneity of variance and a statistical difference in estimated numbers of Reelin-IR neurons between age groups (one-way ANOVA followed by a post hoc Tukey test) using IBM SPSS Statistics (Version 20.0.0.1).

Tissue from human AD-subjects was analyzed for co-localization using brightfield microscopy (Zeiss Axio Imager M1) and focusing through the tissue using a high power objective (100× oil, N.A. 1.4). As we did not have access to complete series of sections through EC, we analyzed all stained neurons rather than doing a stereological analysis on EC-layer II from the available tissue-samples. Consequently, EC-layer II was delineated on each section and all stained neurons were analyzed to determine whether they were positive for Reelin and/or iAβ. Images of human tissue were optimized for color-contrast in ImageJ.

3. Results

3.1. In EC-layer II, iAβ is selectively expressed in Reelin-IR neurons

In the rat transgenic model, immunoenzyme-staining for Reelin and iAβ on separate coronal sections taken from the same level of EC-layer II revealed a highly similar pattern of immunoreactive (IR) neurons for both molecules (Fig. 1A). To test whether Reelin-IR neurons in EC-layer II selectively express iAβ in the transgenic model, we used a double-immunofluorescent staining for both substances, combining a rabbit anti-Reelin antibody with a mouse anti-Aβ (MCSA1) antibody (Fig. 1B). This corroborated the impression of overlap between the two markers while also showing that irrespective of the rostrocaudal level,

Table 1
Overview of primary and secondary antibodies used for rat tissue (top panel) and human tissue (bottom panel). In the case of the rat tissue, corresponding numbers (e.g. 1 and 1′) indicate which primary antibodies were used together in double-labeling experiments shown in the indicated figures.

Antibodies used on rat tissue						
Primary	Rabbit anti-Reelin 1, 2, 3	Mouse anti-Reelin 1′, 4*	Goat anti-Reelin 5	Mouse anti-Aβ (McSA1) 2′, 5′*	Mouse anti-Aβ (MOAB-2) 3′	Rabbit anti-Aβ42 (IBL) 4′
Secondary	Alexa 488 goat anti-rabbit	Alexa 546 goat anti-mouse	Alexa 488 donkey anti-goat	Alexa 546 goat anti-mouse	Alexa 546 goat anti-mouse	
	HRP-conjugated goat anti-rabbit polymer	AP-conjugated goat anti-mouse polymer		AP-conjugated goat anti-mouse polymer		HRP-conjugated goat anti-rabbit polymer

Antibodies used on human tissue		
Primary	Rabbit anti-Reelin	Mouse anti-Aβ (McSA1)
Secondary	HRP-conjugated goat anti-rabbit polymer	AP-conjugated goat anti-mouse polymer

(1 and 1′ Fig. 5A; 2 and 2′ Figs. 1B, 2A–D, 3A, B, 4A, B, 7A, B; 3 and 3′ Figs. 6, 7A, B; 4 and 4′ Fig. 8A, B; 5 and 5′ Fig. 5B; * these antibodies were also used for single labeling, Fig. 1A, C). Fig. 9A, B.

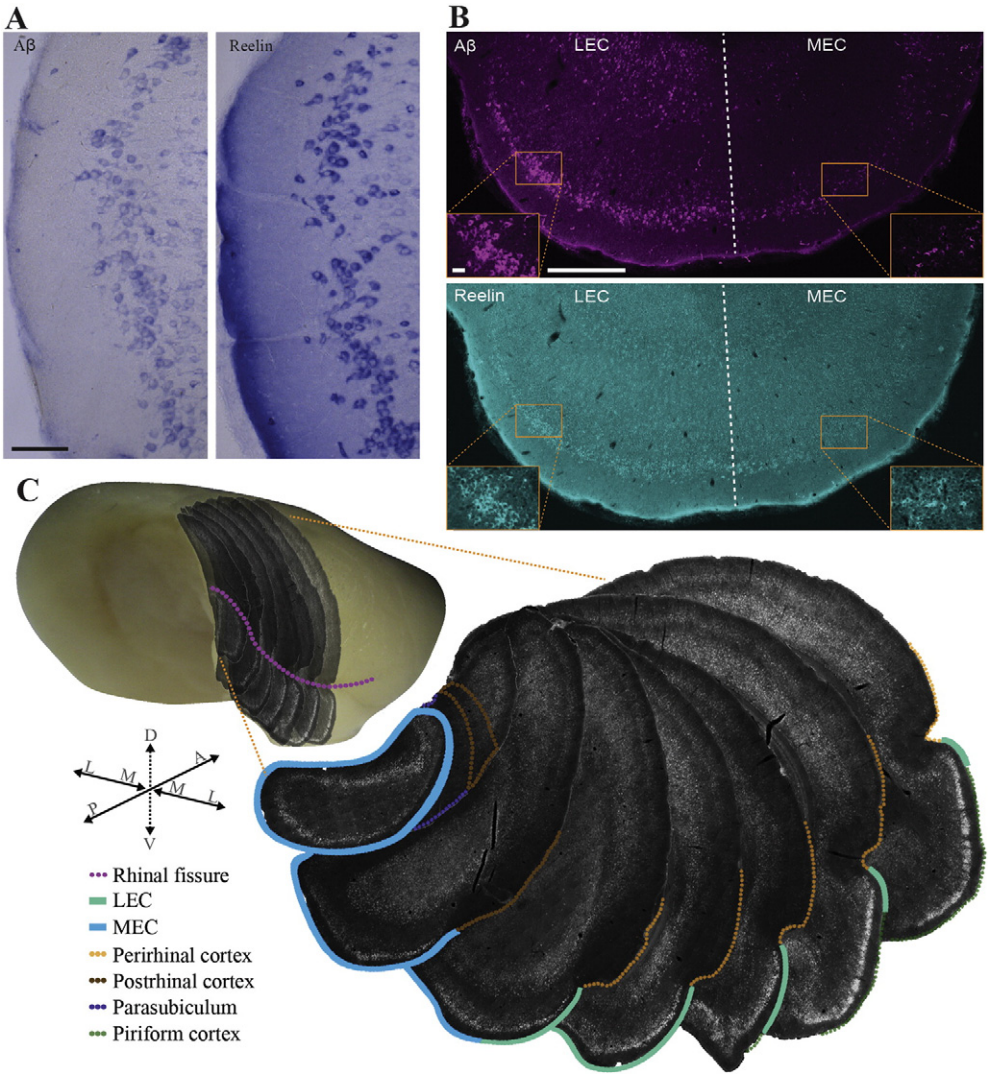

Fig. 1. In EC-layer II iAβ-IR follows the distribution of Reelin-IR and displays a topographical arrangement. (A) Separate immunoenzyme-staining for iAβ (left, McSA1) or Reelin (right, mouse anti-Reelin G10) on sections taken from the same level of EC-layer II produces highly similar patterns. (B) Double-immunofluorescence staining against iAβ (top, McSA1) and Reelin (bottom, rabbit anti-Reelin) reveals virtually identical patterns in EC-layer II. Note that both signals are stronger towards the rhinal fissure (towards the left side of the images). (C) The intensity of iAβ-IR in EC-layer II is topographically distributed. (left) Seven coronal iAβ-immunoreacted sections representative of EC as situated in the rat brain. Position of the rhinal fissure is indicated with a dotted line (magenta). (right) iAβ-immunoreacted sections spread out for better view of EC. In EC-layer II, the highest amount of iAβ-IR material is located towards the rhinal fissure, then gradually drops off when moving away from the rhinal fissure until only a minimal amount is present in the most ventromedial part. LEC and MEC indicated with solid contours; bordering structures indicated with dotted contours. Anatomical compass: A = anterior, P = posterior, D = dorsal, V = ventral, L = lateral, and M = medial. Scale bars: A 100 μm; B, main figures 500 μm, insets 40 μm.

neurons located closer to the rhinal fissure consistently have stronger iAβ- and Reelin-staining than neurons located progressively further away from the rhinal fissure (Fig. 1B, C). In the case of Reelin, this feature has also been noted by others (Perez-Garcia et al., 2001).

To determine the degree of overlap between iAβ-IR and Reelin-IR neurons, we used the double-immunofluorescence staining method and analyzed 5852 neurons in the lateral (LEC) and medial (MEC) subdivisions of EC-layer II (LEC 2114; MEC 3738) from 20 animals divided into four age-groups (P15, 1 month, 3 months and 6 months). The age-groups were selected to start at P15 when adult-like principal neurons are known to be present in EC (Canto and Witter, 2012a, 2012b) and extending up to and including 6 months, thereby covering the pre-plaque stage in our colony of McGill-R-Thy1-APP rats (Heggland et al., 2015). With stereological systematic random sampling, we obtained a reliable estimate of the number of layer II Reelin-IR neurons (P15: LEC 34772, MEC 74710; 1 month: LEC 44558, MEC 116613; 3 months: LEC 52124, MEC 111394; 6 months: LEC 40923, MEC 130129). The estimated Reelin-IR neuron numbers were found normally distributed and with homogeneous variance. Analysis of variance followed by post hoc multiple comparison test (Tukey test), conducted separately for LEC and MEC on all age groups, revealed a significantly lower estimate of Reelin-IR neurons in MEC for the P15 group as compared with MEC-estimates in each of the other three age groups ($P < 0.05$).

In line with our initial observations, the analysis of neurons revealed that iAβ is selectively present in Reelin-IR principal neurons throughout the pre-plaque stage (Fig. 2). In the P15-group, 98.6% of LEC (437/443) and 98.9% of MEC (616/623) Reelin-IR principal neurons in layer II were positive for iAβ (Fig. 2A). For each subsequent age-group we found 100% of Reelin-IR principal neurons in layer II to be immunoreactive for iAβ (Fig. 2B–D). Further, all obtained data combined ($n = 5852$ neurons) showed that only 11 iAβ-IR neurons were not immunoreactive for Reelin; these were found in the P15 ($N = 4$), 3 months ($N = 4$) and the 6 months group ($N = 3$).

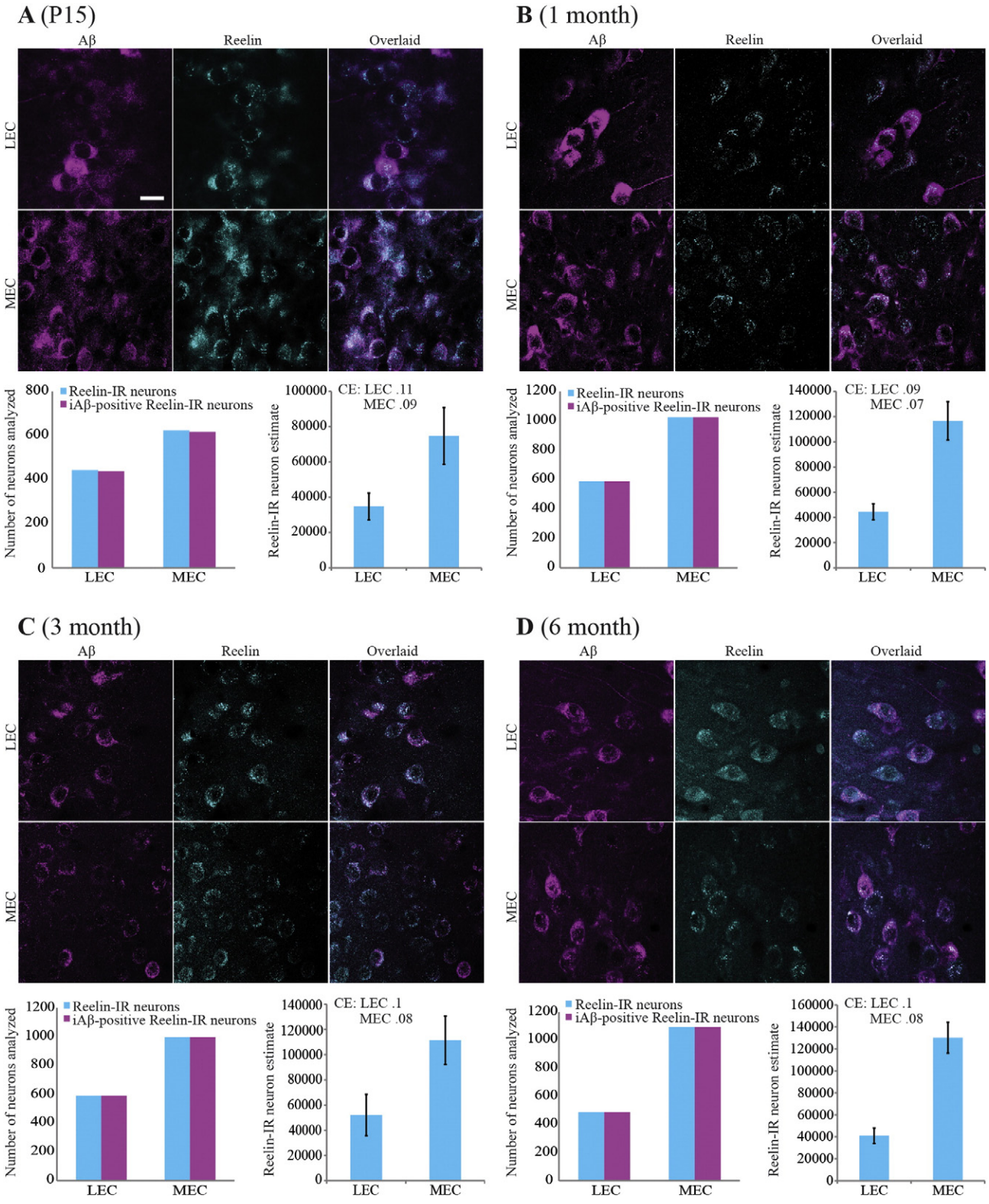

Fig. 2. Analysis of double-immunofluorescence staining in EC-layer II of 20 animals revealed that iAβ-IR material is selectively expressed in Reelin-IR neurons ($n = 5852$ neurons). (A–D) Representative confocal images of iAβ and Reelin-IR neurons in LEC and MEC from double-immunoreacted sections are displayed for ages P15 (A), one month (B), three months (C) and six months (D). For each age-group the number of EC-layer II Reelin-IR principal neurons analyzed, together with the number of these co-localizing with iAβ is shown (lower left). The estimated total population of Reelin-IR neurons in layer II of LEC vs MEC is shown as well (lower right; mean ± standard deviation; CE = coefficient of error). With exception of 13 neurons in the P15 group, every Reelin-IR principal neuron was found positive for iAβ, and, importantly, for all age-groups combined we observed iAβ outside the Reelin-IR population in only 11 instances. Scale bar, 20 μm. Five animals were used for each age-group.

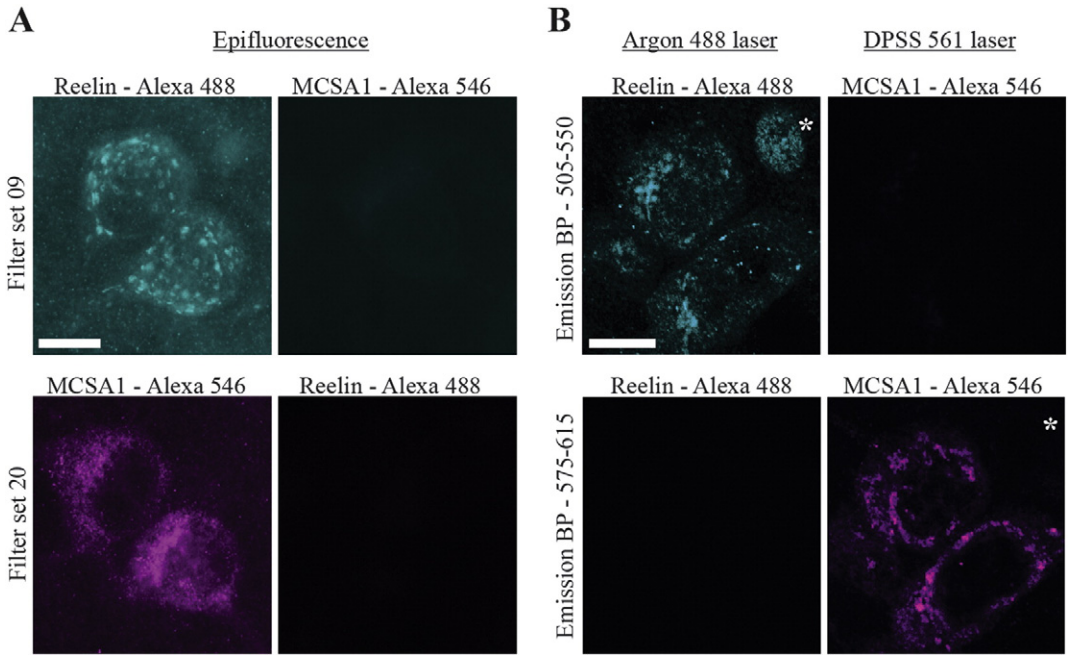

Fig. 3. Absence of bleed-through in both epifluorescence and confocal setup. (A) Epifluorescence microscopical images of single-labeled sections (rabbit anti-Reelin with Alexa 488 and McSA1 with Alexa 546), using the settings used for the analysis, demonstrate absence of bleed-through of signal in the non-matching filter sets. (B) Confocal microscopical analysis of double-labeled sections (rabbit anti-Reelin with Alexa 488 and McSA1 with Alexa 546) and comparison of the emitted signal between the matching and non-matching detection channel for each laser line. No indication of bleed-through between the channels used in our confocal microscope-setup is seen. Note a Reelin-IR interneuron (asterisk) negative for Aβ, serving as an additional control against potential channel bleed-through. Scale bars, 10 μm.

3.2. Control experiments confirm and reinforce iAβ-Reelin association

The observed high incidence of co-localization between Reelin and iAβ is based on fluorescence microscopy of immunoreacted brain sections. This experimental approach suffers from three inherent ways leading to false positive results. First, crosstalk between fluorophores could result if these have overlapping excitation or emission spectra. Second, the rabbit anti-Reelin primary antibody could potentially be unspecific. Third, the mouse anti-Aβ primary antibody (McSA1) could potentially be unspecific. These three possible events were therefore investigated in turn.

For the experiments we used the Alexa 488 dye to image Reelin and the Alexa 546 dye to image iAβ. In order to assess potential spectral bleed-through, we imaged single-immunoreacted sections labeled with either Alexa 488 dye or Alexa 546 dye and compared the emitted signal between the matching and non-matching filters used in our epifluorescence microscope-setup. This procedure revealed no evidence of bleed-through (Fig. 3A). We further tested for bleed-through using

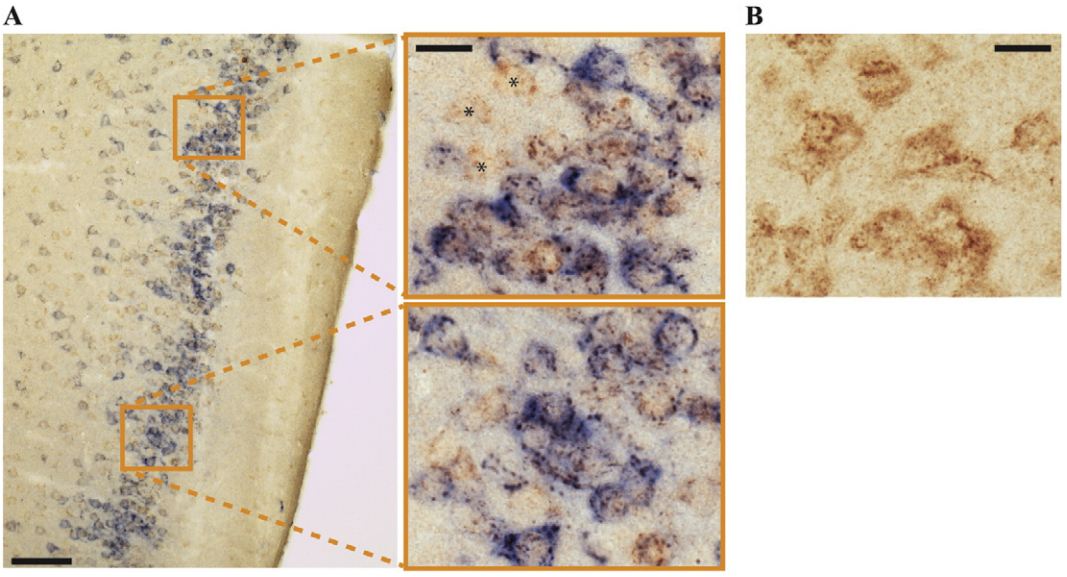

Fig. 4. Double-immunoenzyme staining produced results equivalent to the double-immunofluorescence procedure. (A) EC from 6 month old transgenic rat double-immunoreacted against iAβ (blue; McSA1) and Reelin (brown; rabbit anti-Reelin). The blue reaction product (iAβ) is confined to the vast majority of Reelin-IR layer II neurons; note that three weakly Reelin-IR neurons are negative for iAβ (asterisks). iAβ is not found in non-Reelin-IR neurons. (B) iAβ as detected with McSA1 is absent from Reelin-IR EC-layer II neurons from age-matched controls. Scale bars (A) 100 μm, insets 20 μm (B) 20 μm.

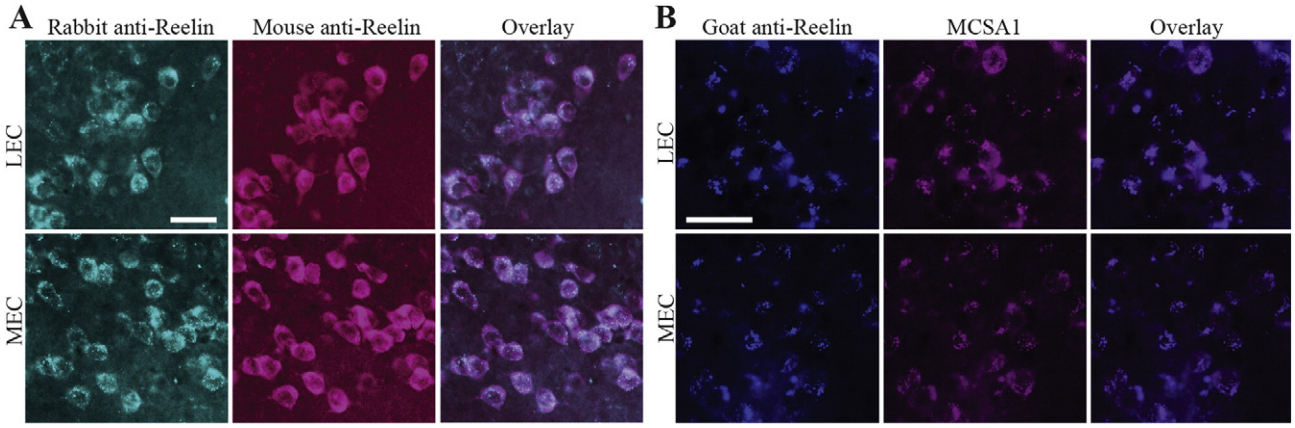

Fig. 5. Specificity of rabbit anti-Reelin antibody corroborated by alternative antibodies. (A) Very high degree of overlap of the rabbit anti-Reelin antibody (Biorbyt) with the well characterized mouse anti-Reelin G10 clone (Millipore) in layer II of both MEC and LEC. (B) Very high degree of overlap of goat anti-Reelin (R&D Systems) with McSA1 which is virtually identical to that obtained with rabbit anti-Reelin (see Figs. 1 and 2). Scale bars, 40 μm.

confocal microscopy by scanning double-immunoreacted sections and comparing the emitted signal between the matching and non-matching detection channel for each laser line. Again, we found no evidence of bleed-through between the channels used in our confocal microscope-setup. In these confocal images, we further observed a Reelin-IR neuron negative for iAβ, providing an additional control against bleed-through (Fig. 3B).

As a control for the double-immunofluorescence method, we performed double-immunoenzyme staining with the same pair of antibodies on sections from 1 and 6 month old transgenic rats vs. controls. This essentially replicated the results of our double-immunofluorescence procedure (Fig 4A, B).

In order to ensure the specificity of the rabbit anti-Reelin antibody, we compared its immunoreactivity with that of the well-characterized mouse anti-Reelin G10 clone in a double-immunostaining procedure. This revealed a near complete overlap between the two antibodies in EC-layer II (Fig. 5A). Additionally, we replaced the rabbit anti-Reelin antibody with a goat anti-Reelin antibody and performed double-immunostaining together with McSA1, which corroborated our original results (Fig. 5B).

As a control for the McSA1 antibody, we replaced it with MOAB-2, an antibody that exclusively binds Aβ-peptides, in particular the Aβ42-form (Youmans et al., 2012). Double-immunofluorescence staining using MOAB-2 and rabbit anti-Reelin again confirmed our original results, i.e. iAβ was selectively associated with Reelin-IR neurons (Fig. 6).

Further, MOAB-2 immunolabeling gave an intracellular pattern strikingly similar to that seen in case of Reelin-IR (Fig. 6, insets). Subsequent confocal microscopy revealed Reelin-IR material partially co-localized with iAβ as detected by McSA1, while a near complete co-localization was observed between Reelin-IR material and iAβ as detected by MOAB-2 (Fig. 7A, B).

Finally, we used a rabbit C-terminal specific antibody against Aβ42 together with the mouse anti-Reelin G10 clone and performed double-immunoenzyme staining on 6 month old animals. This method revealed strong iAβ42 labeling in EC-layer II Reelin-IR neurons in the rat transgenic model vs. controls (Fig. 8).

3.3. Evidence for iAβ-Reelin association in EC of human AD-cases

We next investigated whether the iAβ-Reelin association directly relates to the etiology of AD in humans, by using the MCSA1 and rabbit anti-Reelin antibodies and analyzing double-immunoreacted samples of EC-tissue from three human subjects with pathologically confirmed AD, including Braak stages I, III and V (Fig. 9A, B). Out of 3077 layer II neurons immunoreactive for Reelin across all analyzed samples, 2871 neurons were also immunoreactive for iAβ. Only 36 neurons negative

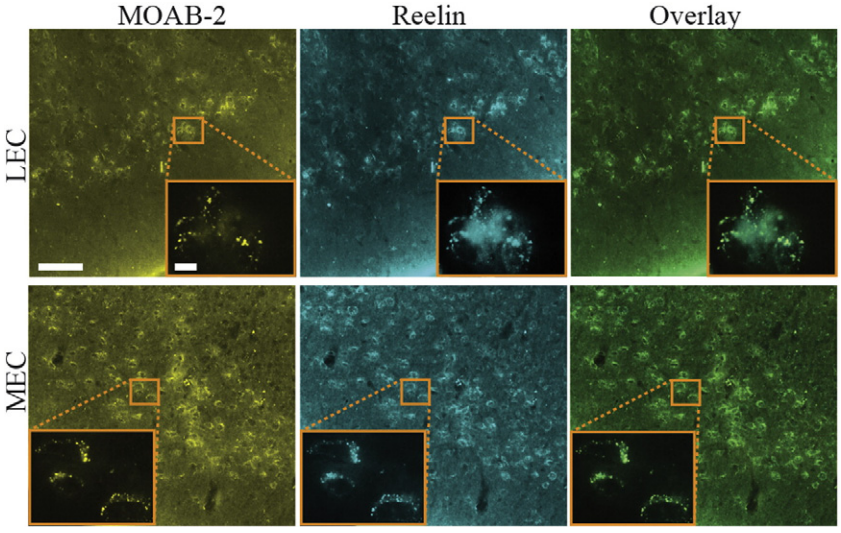

Fig. 6. Aβ42 (detected with a specific antibody, MOAB-2; Biosensis) is confined to Reelin-IR neurons in EC-layer II. Note the high degree of intracellular overlap between Reelin and MOAB-2 staining. Scale bars, 100 μm, inset 10 μm.

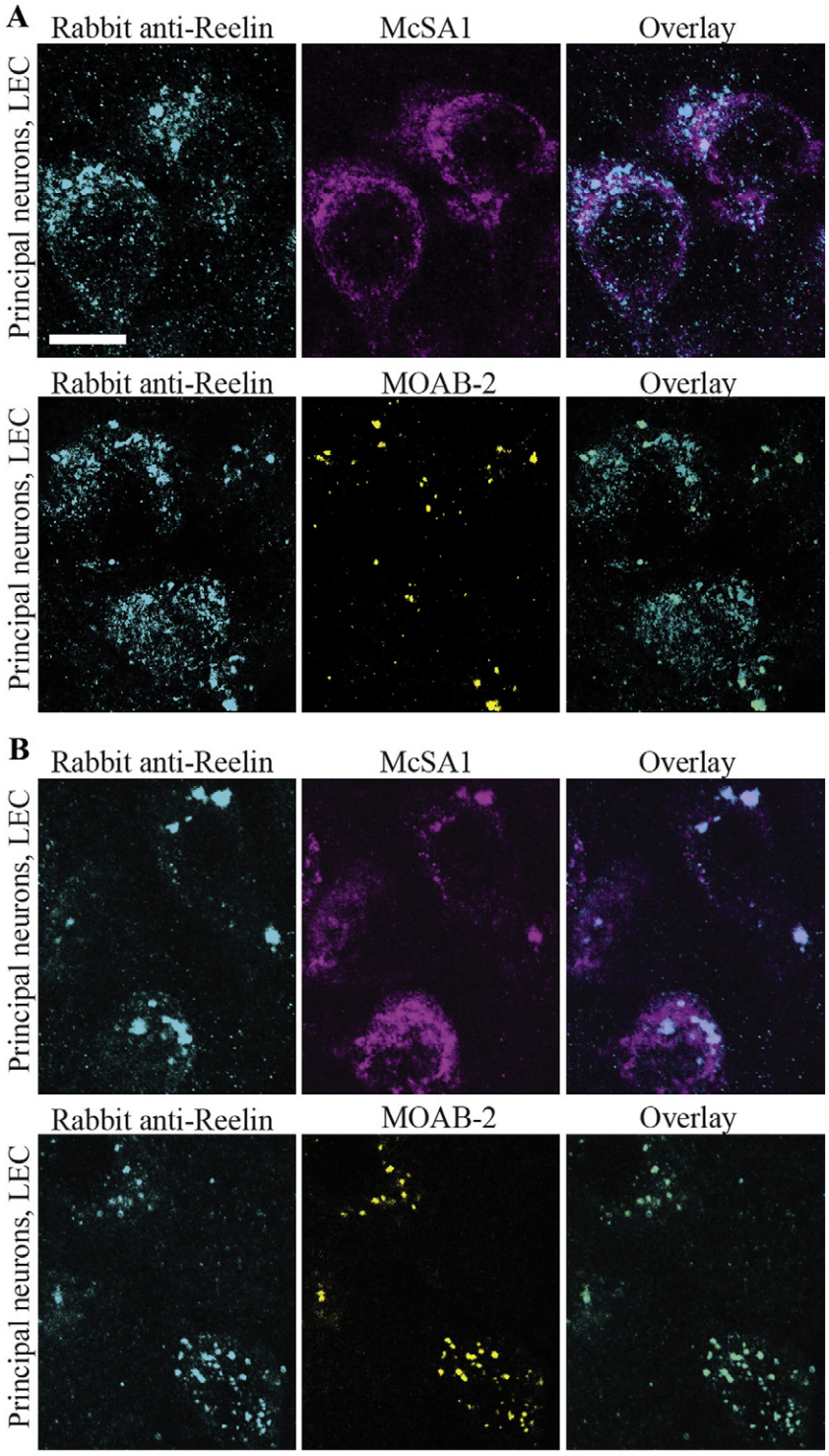

Fig. 7. Intracellular colocalization in granules between MOAB-2 and Reelin immunoreactivity, and McSA1 and Reelin immunoreactivity. The McSA1 and MOAB-2 antibodies both detect iAβ; the latter preferentially binds Aβ42. For both antibodies, confocal analysis shows that immunoreactivity colocalizes with Reelin-IR granules. (A) Example from LEC of a 3 month old rat. (B) Example from LEC of a 6 month old rat. Scale bar, 10 μm.

for Reelin were found to contain iAβ (Fig. 9C). In particular, for Braak stage I, we identified 1631 Reelin-IR neurons in EC-layer II of which 1497 were also iAβ-IR, while 8 Reelin-negative neurons contained iAβ. For Braak stage III, we identified 969 Reelin-IR neurons in EC-layer II of which 950 were also iAβ-IR, while 21 Reelin-negative neurons contained iAβ. For Braak stage V, we identified 441 Reelin-IR neurons in EC-layer II of which 424 were also iAβ-IR, while 7 Reelin-negative neurons contained iAβ.

4. Discussion

We report that in EC-layer II, Reelin-IR neurons selectively express iAβ during the pre-plaque stage in a transgenic rat model for AD, such that essentially no iAβ is found in layer II neurons that do not express Reelin. Further, we present evidence that this may directly translate to the situation in the human brain during the initial pathological stages of AD. Finally, in the rat model we observe a topographical gradient in

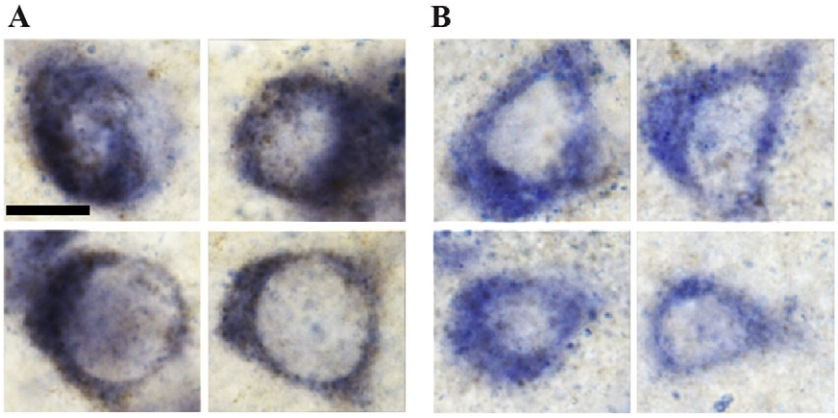

Fig. 8. C-terminal specific Aβ42-antibody confirms expression of iAβ in EC-layer II Reelin positive neurons. (A) Double-immunoenzyme staining on 6 month old transgenic rats using rabbit IBL anti-Aβ42 (dark brown) and mouse anti-Reelin G10 (blue) shows clear presence of iAβ42 in EC-layer II Reelin-IR neurons. (B) Minimal amounts of iAβ42 are detected in EC-layer II Reelin-IR neurons in 6 month old control rats. Scale bar, 10 μm.

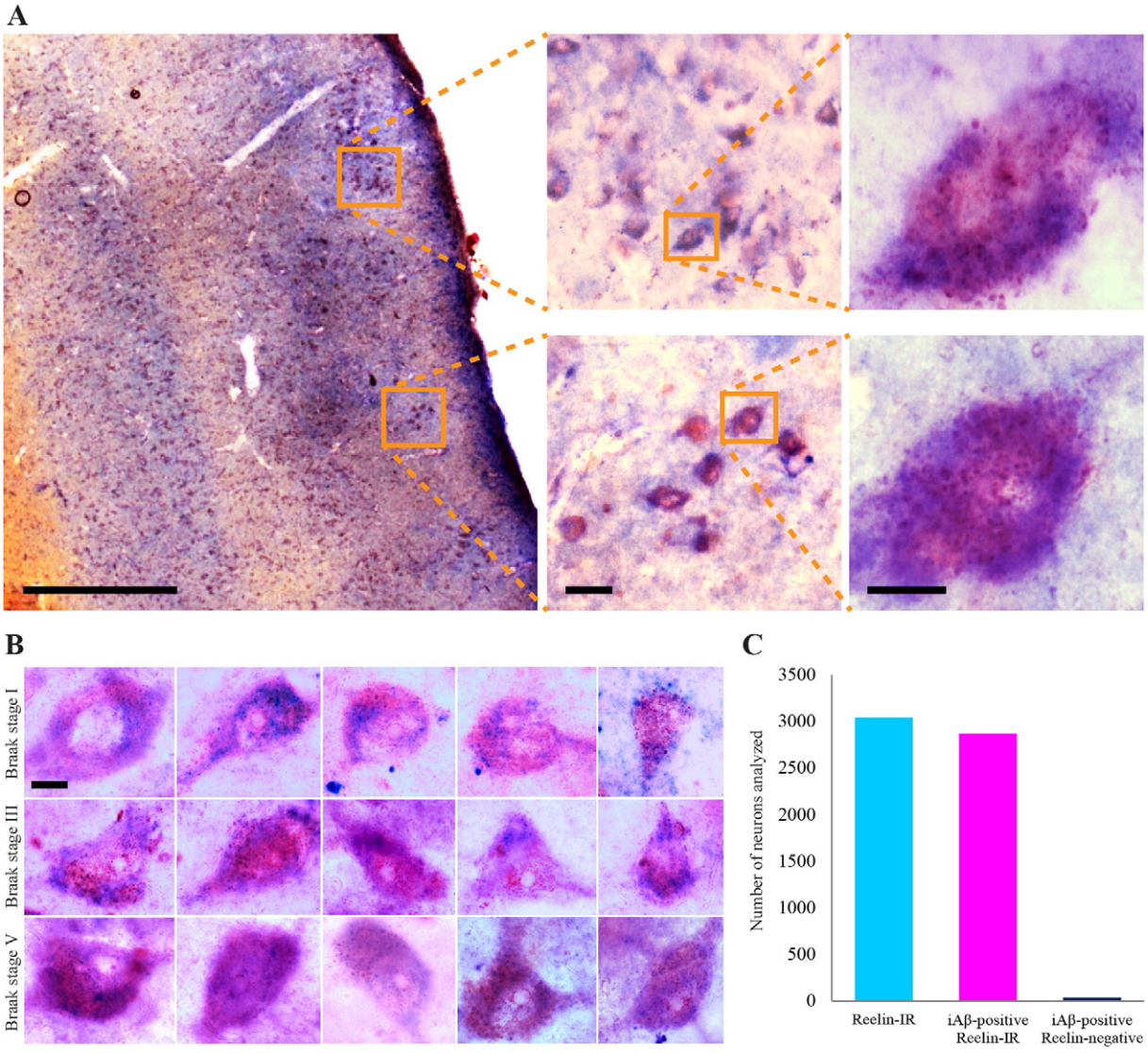

Fig. 9. Strong association of iAβ and Reelin-IR EC-layer II neurons in human subjects diagnosed with AD. (A) Example of EC from subject classified as Braak stage III, where iAβ (blue) is selectively present in Reelin-IR (red) neurons in layer II. Scale bars, left image 500 μm, middle images 40 μm, right images 10 μm. (B) High power micrographs of representative individual EC-layer II Reelin-IR neurons containing iAβ from each of Braak stages I, III and V. Note that in some areas of the intracellular compartment the red and blue chromogens appear to overlap, yielding a purple intermediate. Scale bar, 10 μm. (C) Quantification of neuron types. Out of 3077 EC-layer II Reelin-IR neurons analyzed, 2871 stained positive for iAβ. Conversely, only 36 Reelin-negative neurons stained positive for iAβ. Numbers pr. Braak stage of total Reelin-IR/iAβ-positive Reelin-IR/iAβ-positive Reelin-negative: Braak I, 1631/1497/8; Braak III, 969/950/21; Braak V, 441/424/7.

EC-layer II, with immunoreactivity for iAβ being strongest in neurons located closest to the rhinal fissure.

Immunolabeling as a means to detect Aβ-peptides requires the use of antibodies that are not confounded by exhibiting cross reactivity to APP or its non-Aβ cleavage fragments. For our experiments we used the extensively tested anti-Aβ antibody MCSA1, which has been shown to exhibit minimal cross reactivity with APP as well as the β C-terminal fragment (β-CTF) (Iulita et al., 2014; Leon et al., 2010). We subsequently verified the presence of iAβ in EC-layer II Reelin-IR neurons with the MOAB-2 antibody, which binds Aβ-peptides with a strong preference for Aβ42 without any cross reactivity to APP or β-CTF (Youmans et al., 2012). Finally, we used a C-terminal specific anti-Aβ42 antibody in order to substantiate that elevated levels of Aβ42 is indeed a characteristic of EC-layer II Reelin-IR neurons.

Aβ-peptides have been recognized as important factors in the initiation of AD (Billings et al., 2005; Casas et al., 2004; Choi et al., 2014; Cohen et al., 2013; Iulita et al., 2014; Knobloch et al., 2007; Lambert et al., 1998; Leon et al., 2010; McLean et al., 1999; Naslund et al., 2000; Umeda et al., 2011; Walsh et al., 2002). Neuronal accumulation of iAβ, in particular Aβ42, is an initial event in AD (D'Andrea et al., 2001; Fernandez-Vizarra et al., 2004; Gouras et al., 2000, 2010; Pensalfini et al., 2014), while EC-layer II has been identified as exhibiting early pathological changes, with neuronal loss evident already at preclinical stages (Braak and Braak, 1991; Gomez-Isla et al., 1996; Kordower et al., 2001). Our findings in EC-layer II that iAβ is confined to Reelin-IR neurons, and that Aβ42 and Reelin apparently are co-localized within the cells provide a clear indication that Reelin and iAβ could be structurally associated. This is in line with reports that amyloid-peptides and Reelin co-localize in hippocampal amyloid deposits of aged transgenic and wild-type mice (Doehner et al., 2010) and that Reelin extracted from AD-brains consists of various complexes of higher molecular mass instead of the functional homodimers seen in age-matched controls (Cuchillo-Ibáñez et al., 2013).

Supporting this proposed structural association is a report that in the presence of Aβ42, Reelin fails to form the homodimers, which constitute the active form of Reelin. This results in a reduced ability to activate ApoER2, the main Reelin-receptor in the brain (Cuchillo-Ibáñez et al., 2013). Aβ-induced impairment of Reelin signaling may influence targets downstream of Reelin-IR neurons. Reelin-IR neurons are the exclusive origin of the excitatory projection from EC-layer II onto the hippocampal DG, as well as to the CA2 and CA3 subdivisions (Berndtsson, 2013; Gianatti, 2015; Kitamura et al., 2014; Varga et al., 2010). A substantial proportion of non-Reelin positive neurons in layer II have been identified as being immunoreactive for the calcium binding protein calbindin (Naumann et al., 2015; Varga et al., 2010). Although the functional properties of Reelin positive and calbindin positive neurons in layer II are still enigmatic, it is established that calbindin neurons do not, or sparsely project to HF (Kitamura et al., 2014; Varga et al., 2010).

Reelin, synthesized in EC-layer II, can be transported to and released at its hippocampal targets in a manner independent of neurotransmitter release (Martinez-Cerdeno et al., 2003). The significance of this constitutive release is currently not fully understood, but application of Reelin to the bath fluid of hippocampal slices enhanced long-term potentiation in hippocampal neurons (Qiu et al., 2006; Weeber et al., 2002). Also, injecting Reelin into the ventricles of adult mice resulted in enhanced performance on hippocampus-dependent tasks, and correlated with increased hippocampal dendritic spine density (Rogers et al., 2011). Since axons from EC-layer II neurons projecting to the hippocampus also give rise to an extensive collateral plexus in layers I and II of EC (Canto and Witter, 2012a, 2012b), one may suggest that synaptic alterations similar to those reported in the hippocampus could take place in EC as well. It is important to keep in mind however, that the relationship between Reelin, iAβ, and cognitive functions is not unequivocally established. Nevertheless, if iAβ structurally associates with Reelin in EC-layer II neurons during initial AD-stages, impaired transport of Reelin from these neurons onto their hippocampal synaptic terminals might be expected. In line with this, early (P30) overall loss of Reelin, as measured with western blot, has been reported in the hippocampus of transgenic mice carrying human *APP* with AD-related mutations. Moreover, in human AD-cases, loss of Reelin was found specifically associated with CA3-CA2 neurites corresponding to terminations from EC-layer II neurons (Herring et al., 2012).

We observed the strongest iAβ-IR in EC-layer II neurons located in dorsolateral portions of EC, i.e. close to the rhinal fissure. A topologically comparable preferred expression of hyperphosphorylated tau has been found in EC of a transgenic mouse model and in EC of AD-brains (Braak and Braak, 1991; Khan et al., 2014). In rodents, dorsolateral EC preferentially connects with dorsal parts of the hippocampal formation, while more ventromedial parts of EC connect to ventral parts of the hippocampal formation (Cappaert et al., 2014). This connectional topography is paralleled by gradual differences in resolution of spatial coding in both structures, such that the level of resolution with which the environment is represented changes along their respective dorsoventral axes. In the rodent hippocampal formation, the size of the specific spatial receptive field of place cells increases along the dorsoventral axis (Jung et al., 1994; Kjelstrup et al., 2008). A similar spatial granularity gradient exists in EC, where grid cells close to the rhinal fissure have a fine-grained spatial representation, while cells located progressively further away from the rhinal fissure are tuned to increasingly more coarse spatial representations (Brun et al., 2008; Stensola et al., 2012). An analogous gradient is present in human hippocampal formation and EC, where the most posterior parts correlate with fine-grained spatial representations, while engagement of anterior parts reflect coarse-grained spatial representations (Evensmoen et al., 2013, 2015). Taken together, these findings logically imply that initial iAβ-induced impairment of entorhinal-hippocampal connectivity is likely to selectively affect functions associated with fine-grained representations of external information. This interpretation concurs with navigational deficits that are already evident in subjects with mild cognitive impairment (Hort et al., 2007; Laczo et al., 2009), as well as with the recently reported predictive sensitivity of fine grained recall tasks as part of the diagnostic criteria for early diagnosis of AD (Dubois et al., 2014).

5. Conclusions

Although we only analyzed a small sample of human AD cases, the consistency of the human observations about the selective presence of iAβ in EC-layer II Reelin-IR neurons is evident, suggesting that this might be a common feature of human AD-pathology. This is supported by the more extensive, consistent rat-model data, where selective presence of iAβ in Reelin-IR neurons in EC-layer II is evident throughout the pre-plaque stage. However, a study on a larger sample of human AD-cases is needed in order to substantiate that selective presence of iAβ in Reelin-IR neurons in EC-layer II is indeed a shared feature in AD patients, and whether or not this association in the early stage of the disease selectively occurs in those parts of EC which are adjacent to the rhinal and collateral sulci. If so, this will emphasize that a structural interaction between Reelin and iAβ indeed is a crucial factor in the etiology of AD, forming a signature of early disease-stages. This may lead to refined hypotheses concerning disease-initiating mechanisms and eventually to the development of targeted treatments of AD.

Competing interests

The authors declare that they have no competing interests.

Funding

This study was supported by a grant from the Central Norway Regional Health Authority (# 46056620), the Kavli Foundation, and the

Norwegian Research Council Centre of Excellence and Equipment Grants (# 145993, 181676).

Contributions

AK-F and MPW conceived and designed the study, AK-F and AN collected the data and did the data-analysis, while AK-F and MPW wrote the manuscript.

Acknowledgments

We acknowledge the help of Ingrid Heggland and Hanne Soligard for the breeding and genotyping of the AD-transgenic rats, and the help of Bruno Monterotti and Ingunn Nervik with histological procedures. We thank Prof. Sverre Torp at the Department of Laboratory Medicine, St. Olavs Hospital, Norway, for advice on how to handle immunostaining of human brain tissue as well as valuable discussions and input concerning the neuropathology of AD. We would also like to thank Prof. Ricardo Insausti, University of Castilla-La Mancha, Spain, for generously providing us with samples of human AD-brain tissue. Finally, we very much appreciate the constructive feedback obtained from Dr. Edvard Moser.

References

Arriagada, P.V., Growdon, J.H., Hedley-Whyte, E.T., Hyman, B.T., 1992. Neurofibrillary tangles but not senile plaques parallel duration and severity of Alzheimer's disease. Neurology 42, 631-631. http://dx.doi.org/10.1212/WNL.42.3.631.

Berndtsson, C., 2013. The specificity of output from medial entorhinal cortex (Master's thesis) Department of Neuroscience. Norwegian University of Science and Technology, Trondheim.

Billings, L.M., Oddo, S., Green, K.N., McGaugh, J.L., LaFerla, F.M., 2005. Intraneuronal Abeta causes the onset of early Alzheimer's disease-related cognitive deficits in transgenic mice. Neuron 45, 675–688. http://dx.doi.org/10.1016/j.neuron. 2005.01.040.

Braak, H., Braak, E., 1991. Neuropathological stageing of Alzheimer-related changes. Acta Neuropathol. 82, 239–259. http://dx.doi.org/10.1007/BF00308809.

Brun, V.H., Solstad, T., Kjelstrup, K.B., Fyhn, M., Witter, M.P., Moser, E.I., Moser, M.B., 2008. Progressive increase in grid scale from dorsal to ventral medial entorhinal cortex. Hippocampus 18, 1200–1212. http://dx.doi.org/10.1002/hipo.20504.

Canto, C.B., Witter, M.P., 2012a. Cellular properties of principal neurons in the rat entorhinal cortex. I. The lateral entorhinal cortex. Hippocampus 22, 1256–1276. http://dx.doi.org/10.1002/hipo.20997.

Canto, C.B., Witter, M.P., 2012b. Cellular properties of principal neurons in the rat entorhinal cortex. II. The medial entorhinal cortex. Hippocampus 22, 1277–1299. http://dx.doi.org/10.1002/hipo.20993.

Cappaert, N.L.M., Van Strien, N.M., Witter, M.P., 2014. Hippocampal formation. In: Paxinos, G. (Ed.), The Rat Brain, 4 ed. Elsevier Academic Press, San Diego, CA, US; London, UK, pp. 511–574 http://dx.doi.org/10.1016/B978–0–12–374245-2.00020-6.

Casas, C., et al., 2004. Massive CA1/2 neuronal loss with intraneuronal and *N*-terminal truncated abeta 42 accumulation in a novel Alzheimer transgenic model. Am. J. Pathol. 165, 1289–1300. http://dx.doi.org/10.1016/S0002-9440(10)63388-3.

Chin, J., et al., 2007. Reelin depletion in the entorhinal cortex of human amyloid precursor protein transgenic mice and humans with Alzheimer's disease. J. Neurosci. 27, 2727–2733. http://dx.doi.org/10.1523/JNEUROSCI.3758-06.2007.

Choi, S.H., et al., 2014. A three-dimensional human neural cell culture model of Alzheimer's disease. Nature 515, 274–278. http://dx.doi.org/10.1038/nature 13800.

Cohen, R.M., et al., 2013. A transgenic Alzheimer rat with plaques, tau pathology, behavioral impairment, oligomeric Abeta, and frank neuronal loss. J. Neurosci. 33, 6245–6256. http://dx.doi.org/10.1523/JNEUROSCI.3672-12.2013.

Cuchillo-Ibáñez, I., Balmaceda, V., Botella-López, A., Rabano, A., Avila, J., Sáez-Valero, J., 2013. Beta-amyloid impairs reelin signaling. PLoS One 8. http://dx.doi.org/10.1371/journal.Pone.0072297.

D'Andrea, M.R., Nagele, R.G., Wang, H.Y., Peterson, P.A., Lee, D.H., 2001. Evidence that neurones accumulating amyloid can undergo lysis to form amyloid plaques in Alzheimer's disease. Histopathology 38, 120–134 (doi: his 1082 [pii]).

Doehner, J., Madhusudan, A., Konietzko, U., Fritschy, J.M., Knuesel, I., 2010. Co-localization of reelin and proteolytic Abeta PP fragments in hippocampal plaques in aged wild-type mice. J. Alzheimers Dis. 19, 1339–1357. http://dx.doi.org/10.3233/JAD-2010-1333.

Dubois, B., et al., 2014. Advancing research diagnostic criteria for Alzheimer's disease: the IWG-2 criteria. Lancet Neurol. 13, 614–629. http://dx.doi.org/10.1016/S1474-4422(14)70090-0.

Duyckaerts, C., Delatour, B., Potier, M.C., 2009. Classification and basic pathology of Alzheimer disease. Acta Neuropathol. 118, 5–36. http://dx.doi.org/10.1007/s00401-009-0532-1.

Espinosa, A., et al., 2013. A longitudinal follow-up of 550 mild cognitive impairment patients: evidence for large conversion to dementia rates and detection of major risk factors involved. J. Alzheimers Dis. 34, 769–780. http://dx.doi.org/10.3233/JAD-122002.

Evensmoen, H.R., Lehn, H., Xu, J., Witter, M.P., Nadel, L., Haberg, A.K., 2013. The anterior hippocampus supports a coarse, global environmental representation and the posterior hippocampus supports fine-grained, local environmental representations. J. Cogn. Neurosci. 25, 1908–1925. http://dx.doi.org/10.1162/jocn_a_00436.

Evensmoen, H.R., Ladstein, J., Hansen, T.I., Moller, J.A., Witter, M.P., Nadel, L., Haberg, A.K., 2015. From details to large scale: the representation of environmental positions follows a granularity gradient along the human hippocampal and entorhinal anterior–posterior axis. Hippocampus 25, 119–135. http://dx.doi.org/10.1002/hipo.22357.

Fernandez-Vizarra, P., et al., 2004. Intra- and extracellular Abeta and PHF in clinically evaluated cases of Alzheimer's disease. Histol. Histopathol. 19, 823–844.

Gianatti, M., 2015. Projections of calbindin expressing neurons in layer II of the entorhinal cortex (Master's Thesis) Norwegian University of Science and Technology, Trondheim.

Gomez-Isla, T., Price, J.L., McKeel Jr., D.W., Morris, J.C., Growdon, J.H., Hyman, B.T., 1996. Profound loss of layer II entorhinal cortex neurons occurs in very mild Alzheimer's disease. J. Neurosci. 16, 4491–4500.

Gouras, G.K., et al., 2000. Intraneuronal Abeta 42 accumulation in human brain. Am. J. Pathol. 156, 15–20. http://dx.doi.org/10.1016/S0002-9440(10)64700-1.

Gouras, G.K., Tampellini, D., Takahashi, R.H., Capetillo-Zarate, E., 2010. Intraneuronal beta-amyloid accumulation and synapse pathology in Alzheimer's disease. Acta Neuropathol. 119, 523–541. http://dx.doi.org/10.1007/s00401-010-0679-9.

Grundman, M., et al., 2004. Mild cognitive impairment can be distinguished from Alzheimer disease and normal aging for clinical trials. Arch. Neurol. 61, 59–66. http://dx.doi.org/10.1001/archneur.61.1.59.

Heggland, I., Storkaas, I.S., Soligard, H.T., Kobro-Flatmoen, A., Witter, M.P., 2015. Stereological estimation of neuron number and plaque load in the hippocampal region of a transgenic rat model of Alzheimer's disease. Eur. J. Neurosci. 41, 1245–1262. http://dx.doi.org/10.1111/ejn.12876.

Herring, A., et al., 2012. Reelin depletion is an early phenomenon of Alzheimer's pathology. J. Alzheimer. Dis. 30, 963–979. http://dx.doi.org/10.3233/Jad-2012-112069.

Hort, J., Laczo, J., Vyhnalek, M., Bojar, M., Bures, J., Vlcek, K., 2007. Spatial navigation deficit in amnestic mild cognitive impairment. Proc. Natl. Acad. Sci. U. S. A. 104, 4042–4047. http://dx.doi.org/10.1073/pnas.0611314104.

Hyman, B.T., Trojanowski, J.Q., 1997. Consensus recommendations for the postmortem diagnosis of Alzheimer disease from the National Institute on Aging and the Reagan Institute Working Group on diagnostic criteria for the neuropathological assessment of Alzheimer disease. J. Neuropathol. Exp. Neurol. 56, 1095–1097. http://dx.doi.org/10.1016/S0197-4580(97)00057-2.

Iulita, M.F., et al., 2014. Intracellular Abeta pathology and early cognitive impairments in a transgenic rat overexpressing human amyloid precursor protein: a multidimensional study. Acta Neuropathol. Commun. 2, 61. http://dx.doi.org/10.1186/2051-5960-2-61.

Jung, M.W., Wiener, S.I., McNaughton, B.L., 1994. Comparison of spatial firing characteristics of units in dorsal and ventral hippocampus of the rat. J. Neurosci. 14, 7347–7356.

Khan, U.A., et al., 2014. Molecular drivers and cortical spread of lateral entorhinal cortex dysfunction in preclinical Alzheimer's disease. Nat. Neurosci. 17, 304–311. http://dx.doi.org/10.1038/nn.3606.

Kitamura, T., Pignatelli, M., Suh, J., Kohara, K., Yoshiki, A., Abe, K., Tonegawa, S., 2014. Island cells control temporal association memory. Science 343, 896–901. http://dx.doi.org/10.1126/science.1244634.

Kjelstrup, K.B., et al., 2008. Finite scale of spatial representation in the hippocampus. Science 321, 140–143. http://dx.doi.org/10.1126/science. 1157086.

Kjonigsen, L.J., Leergaard, T.B., Witter, M.P., Bjaalie, J.G., 2011. Digital atlas of anatomical subdivisions and boundaries of the rat hippocampal region. Front. Neuroinform. 5, 2. http://dx.doi.org/10.3389/fninf.2011.00002.

Knobloch, M., Konietzko, U., Krebs, D.C., Nitsch, R.M., 2007. Intracellular Abeta and cognitive deficits precede beta-amyloid deposition in transgenic arcAbeta mice. Neurobiol. Aging 28, 1297–1306. http://dx.doi.org/10.1016/j.neurobiolaging.2006.06.019.

Kordower, J.H., Chu, Y., Stebbins, G.T., DeKosky, S.T., Cochran, E.J., Bennett, D., Mufson, E.J., 2001. Loss and atrophy of layer II entorhinal cortex neurons in elderly people with mild cognitive impairment. Ann. Neurol. 49, 202–213. http://dx.doi.org/10.1002/1531-8249(20010201)49:2<202::AID-ANA40>3.0.CO;2-3.

Laczo, J., et al., 2009. Spatial navigation testing discriminates two types of amnestic mild cognitive impairment. Behav. Brain Res. 202, 252–259. http://dx.doi.org/10.1016/j.bbr.2009.03.041.

Lambert, M.P., et al., 1998. Diffusible, nonfibrillar ligands derived from Abeta1-42 are potent central nervous system neurotoxins. Proc. Natl. Acad. Sci. U. S. A. 95, 6448–6453.

Leon, W., et al., 2010. A novel transgenic rat model with a full Alzheimer's-like amyloid pathology displays pre-plaque intracellular amyloid-associated cognitive impairment. J. Alzheimers Dis. 20, 113–126. http://dx.doi.org/10.3233/JAD-2010-1349.

Livak, K.J., Schmittgen, T.D., 2001. Analysis of relative gene expression data using real-time quantitative PCR and the $2-\Delta\Delta CT$ method. Methods 25, 402–408. http://dx.doi.org/10.1006/meth.2001.1262.

Martinez-Cerdeno, V., Galazo, M.J., Clasca, F., 2003. Reelin-immunoreactive neurons, axons, and neuropil in the adult ferret brain: evidence for axonal secretion of reelin in long axonal pathways. J. Comp. Neurol. 463, 92–116. http://dx.doi.org/10.1002/cne.10748.

McLean, C., et al., 1999. Soluble pool of Aβ amyloid as a determinant of severity of neurodegeneration in Alzheimer's disease. Ann. Neurol. 46, 860–866. http://dx.doi.org/10.1002/1531-8249(199912)46:6<860::AID-ANA8>3.0.CO;2-M.

Naslund, J., Haroutunian, V., Mohs, R., Davis, K., Davies, P., Greengard, P., Buxbaum, J., 2000. Correlation between elevated levels of amyloid-β peptide in the brain and cognitive decline. JAMA 283, 1571–1577. http://dx.doi.org/10.1001/jama.283.12.1571.

Naumann, R.K., Ray, S., Prokop, S., Las, L., Heppner, F.L., Brecht, M., 2015. Conserved size and periodicity of pyramidal patches in layer 2 of medial/caudal entorhinal cortex. J. Comp. Neurol. 524, 783–806. http://dx.doi.org/10.1002/cne.23865.

Pensalfini, A., et al., 2014. Intracellular amyloid and the neuronal origin of Alzheimer neuritic plaques. Neurobiol. Dis. 71, 53–61. http://dx.doi.org/10.1016/j.nbd.2014.07.011.

Perez-Garcia, C.G., Gonzalez-Delgado, F.J., Suarez-Sola, M.L., Castro-Fuentes, R., Martin-Trujillo, J.M., Ferres-Torres, R., Meyer, G., 2001. Reelin-immunoreactive neurons in the adult vertebrate pallium. J. Chem. Neuroanat. 21, 41–51 (doi: S0891061800001046 [pii]).

Pesold, C., Impagnatiello, F., Pisu, M., Uzunov, D., Costa, E., Guidotti, A., Caruncho, H., 1998. Reelin is preferentially expressed in neurons synthesizing γ-aminobutyric acid in cortex and hippocampus of adult rats. Proc. Natl. Acad. Sci. 95, 3221–3226.

Qiu, S., Zhao, L.F., Korwek, K.M., Weeber, E.J., 2006. Differential reelin-induced enhancement of NMDA and AMPA receptor activity in the adult hippocampus. J. Neurosci. 26, 12943–12955. http://dx.doi.org/10.1523/JNEUROSCI.2561-06.2006.

Ramos-Moreno, T., Galazo, M.J., Porrero, C., Martinez-Cerdeno, V., Clasca, F., 2006. Extracellular matrix molecules and synaptic plasticity: immunomapping of intracellular and secreted reelin in the adult rat brain. Eur. J. Neurosci. 23, 401–422. http://dx.doi.org/10.1111/j.1460-9568.2005.04567.x.

Rogers, J.T., et al., 2011. Reelin supplementation enhances cognitive ability, synaptic plasticity, and dendritic spine density. Learn. Mem. 18, 558–564. http://dx.doi.org/10.1101/lm.2153511.

Scheff, S.W., Price, D.A., Schmitt, F.A., Mufson, E.J., 2006. Hippocampal synaptic loss in early Alzheimer's disease and mild cognitive impairment. Neurobiol. Aging 27, 1372–1384. http://dx.doi.org/10.1016/j.neurobiolaging.2005.09.012.

Stensola, H., Stensola, T., Solstad, T., Froland, K., Moser, M.B., Moser, E.I., 2012. The entorhinal grid map is discretized. Nature 492, 72–78. http://dx.doi.org/10.1038/nature11649.

Thal, D.R., et al., 2000. Sequence of Abeta-protein deposition in the human medial temporal lobe. J. Neuropathol. Exp. Neurol. 59, 733–748.

Umeda, T., Tomiyama, T., Sakama, N., Tanaka, S., Lambert, M.P., Klein, W.L., Mori, H., 2011. Intraneuronal amyloid beta oligomers cause cell death via endoplasmic reticulum stress, endosomal/lysosomal leakage, and mitochondrial dysfunction in vivo. J. Neurosci. Res. 89, 1031–1042. http://dx.doi.org/10.1002/jnr.22640.

Varga, C., Lee, S.Y., Soltesz, I., 2010. Target-selective GABAergic control of entorhinal cortex output. Nat. Neurosci. 13, 822–824. http://dx.doi.org/10.1038/nn.2570.

Walsh, D.M., et al., 2002. Naturally secreted oligomers of amyloid beta protein potently inhibit hippocampal long-term potentiation in vivo. Nature 416, 535–539. http://dx.doi.org/10.1038/416535a.

Weeber, E.J., Beffert, U., Jones, C., Christian, J.M., Forster, E., Sweatt, J.D., Herz, J., 2002. Reelin and ApoE receptors cooperate to enhance hippocampal synaptic plasticity and learning. J. Biol. Chem. 277, 39944–39952. http://dx.doi.org/10.1074/jbc.M205147200.

West, M.J., Slomianka, L., Gundersen, H.J.G., 1991. Unbiased stereological estimation of the total number of neurons in the subdivisions of the rat hippocampus using the optical fractionator. Anat. Rec. 231, 482–497. http://dx.doi.org/10.1002/ar.1092310411.

Youmans, K.L., et al., 2012. Intraneuronal abeta detection in 5xFAD mice by a new Abeta-specific antibody. Mol. Neurodegener. 7, 8. http://dx.doi.org/10.1186/1750-1326-7-8.